J. Fluid Mech. (1984), *vol.* 144, *pp.* 403–418
Printed in Great Britain

Flow in a differentially rotated cylindrical drop at moderate Reynolds number

By GEORGE M. HARRIOTT AND ROBERT A. BROWN

Department of Chemical Engineering and Material Processing Center, Massachusetts Institute of Technology, Cambridge, MA 02139

(Received 16 May 1983 and in revised form 15 February 1984)

Galerkin finite-element approximations are combined with computer-implemented perturbation methods for tracking families of solutions to calculate the steady axisymmetric flows in a differentially rotated cylindrical drop as a function of Reynolds number Re, drop aspect ratio and the rotation ratio between the two end disks. The flows for Reynolds numbers below 100 are primarily viscous and reasonably described by an asymptotic analysis. When the disks are exactly counter-rotated, multiple steady flows are calculated that bifurcate to higher values of Re from the expected solution with two identical secondary cells stacked symmetrically about the axial midplane. The new flows have two cells of different size and are stable beyond the critical value Re_c. The slope of the locus of Re_c for drops with aspect ratio up to 3 disagrees with the result for two disks of infinite radius computed assuming the similarity form of the velocity field. Changing the rotation ratio from exact counter-rotation ruptures the junction of the multiple flow fields into two separated flow families.

1. Introduction

The cellular flows induced by differentially rotating two coaxial and parallel solid surfaces that cap a cylindrical drop are of much interest as a fluid-mechanical model for a small-scale floating zone system. In a previous paper (Harriott & Brown 1983; hereinafter referred to as I), we presented an asymptotic analysis for the structure of these flows valid when the Reynolds number Re was small and when surface tension was large enough that capillary pressure dominated viscous stress, so that the zone remained nearly cylindrical for all amounts of differential rotation. The explicit form of the velocity field derived in I allowed detailed analysis of the structure of the flow field for zones of different aspect ratio and the entire range of rotation ratios $-1 \leqslant s \leqslant 1$, where $s \equiv \Omega_2/\Omega_1$ is the ratio of rotation rates of the top (Ω_2) to the bottom (Ω_1) solid surfaces. The flows were classified by the cellular form of the meridional motions driven by the inertial coupling with the imposed angular velocity. These secondary flows varied in structure from a single cell for $s = 0$ to two equal cells symmetric about the midplane of the drop for equal counter-rotation ($s = -1$).

The range of applicability in terms of Re of the asymptotic results in I is undecided and is necessary for establishing their usefulness. Only Kobayashi & Wilcox (1982) present calculations at large Reynolds number; but their finite-difference results are limited to a drop twice as long as its radius with $Re = 100$ and are insufficient for determining the accuracy of the asymptotic formula. In this paper we analyse the structure of the flow fields in exactly cylindrical floating zones for rotation ratios

between $-1 \leqslant s \leqslant 0$ and Reynolds numbers up to 200. To do this, Galerkin finite-element approximations for the velocity and pressure fields are combined with computer-implemented perturbation methods for tracking families of flows to calculate the steady axisymmetric flows with varying Reynolds number for set values of s and aspect ratio.

The numerical methods used here for detecting bifurcations between families of flows and for tracking flow families through turns with respect to Reynolds number are necessary for careful analysis of a nonlinear boundary-value problem. This is especially true of this rotating flow, because of its relationship to the flow between two rotating disks of infinite extent. Starting with Pearson (1965), a number of authors (Mellor *et al.* 1968; Nguyen, Ribault & Florent 1975; Roberts & Shipman 1976; Holodniok, Kubiček & Hlavaček 1981; Szeto 1978; Keller & Szeto 1980) have reported multiple steady-state flows when the velocity field is written in terms of von Kármán's (1921) similarity transformation and no boundary conditions are included at the edge of the disks. Most recently, Szeto (1978; see also Keller & Szeto 1980) used systematic methods for tracking solution families similar to those employed here to calculate 18 different types of flows for various values of s and Re.

Only when the surfaces were exactly counter-rotated ($s = -1$) were a pair of these flow families found to be connected at a bifurcation point in Reynolds number. At this critical value $\widehat{Re}_c$ the family of flows with two symmetric secondary toroidal cells lost stability to bifurcating motions without this plane of symmetry and then evolved to larger values of Reynolds number. Changing the rotation ratio away from $s = -1$ destroyed the symmetry between the rotating surfaces and broke the connecting families into two separate branches. The structure of these flows for s close to -1 is described by the theory of imperfect bifurcations near (in the parameter space) a supercritical bifurcation point (Keener & Keller 1973; Matkowsky & Reiss 1977) and is discussed in §4.2 as it applied to flows in a cylindrical drop.

The finite-element formulation of the governing equations is sketched in §2, and the form of the velocity field for $0 \leqslant Re \leqslant 100$ is described in §3. Results for the multiplicity of the steady flows satisfying the entire set of equations and boundary conditions for the cylindrical drop are presented in §4.

2. Formulation and solution methods

The cylindrical drop of a Newtonian liquid is held between two circular solid surfaces of radius R which are separated by a distance H, as shown in figure 1. The velocity and pressure fields within the drop are written in a stationary dimensionless coordinate system defined by scaling all distances with H so that the drop shape is described solely by the aspect ratio $\Lambda \equiv R/H$. The axisymmetric swirling flows caused by rotating the lower face at a speed Ω and the top at $s\Omega$ are governed by the dimensionless equations of continuity and motion

$$\nabla \cdot \boldsymbol{v} = 0, \tag{1}$$

$$Re\, \boldsymbol{v} \cdot \nabla \boldsymbol{v} + \nabla p - \nabla \cdot \boldsymbol{\tau} = \boldsymbol{0}, \tag{2}$$

in which the velocity has been scaled with ΩR and the pressure with $\mu\Omega\Lambda$, where μ is the liquid viscosity. The Reynolds number is defined by $Re \equiv \rho\Omega RH/\mu$, where ρ is the density of the liquid and $\boldsymbol{\tau} \equiv \frac{1}{2}(\nabla \boldsymbol{v} + \nabla \boldsymbol{v}^{\mathrm{T}})$ is the dimensionless deviatoric stress.

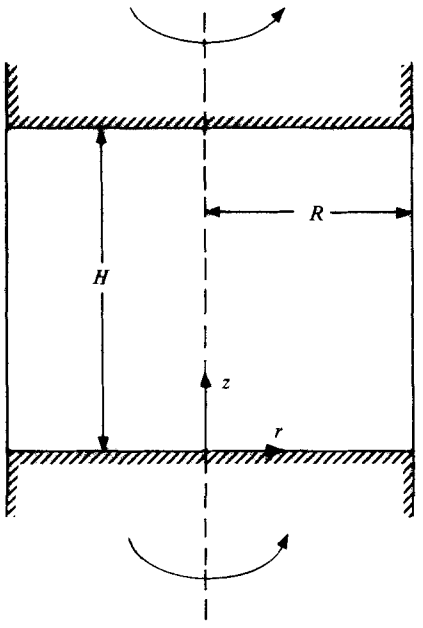

FIGURE 1. A differentially rotated cylindrical drop with radius R and height H.

The boundary conditions on velocity are

$$v_r = 0, \quad v_\theta = 0, \quad \frac{\partial v_z}{\partial r} = 0 \quad (r = 0,\ 0 \leqslant z \leqslant 1), \tag{3}$$

$$v_r = 0, \quad \frac{\partial v_\theta}{\partial r} - \frac{v_\theta}{r} = 0, \quad \frac{\partial v_z}{\partial r} = 0 \quad (r = \Lambda,\ 0 \leqslant z \leqslant 1), \tag{4}$$

$$v_r = 0, \quad v_\theta = r, \quad v_z = 0 \quad (0 \leqslant r \leqslant \Lambda,\ z = 0), \tag{5}$$

$$v_r = 0, \quad v_\theta = sr, \quad v_z = 0 \quad (0 \leqslant r \leqslant \Lambda,\ z = 1). \tag{6}$$

Equations (3) state the standard symmetry conditions for the centerline and (4) are the relations for no penetration and no tangential stress at the cylindrical meniscus. Equations (5) and (6) specify no slip and no penetration along the solid disks.

The flows satisfying (1)–(6) are calculated by the Galerkin finite-element method which is well-developed for the solution of moderate-Reynolds-number Newtonian flows. Since the details of this approach are available in many references (Huyakorn *et al.* 1978; Thomasset 1981), we only sketch the methods used in our calculations. The fluid domain ($0 \leqslant r \leqslant \Lambda, 0 \leqslant z \leqslant 1$) is divided into quadrilateral subdomains or elements and the pressure and velocity fields are approximated by expansions in terms of coefficients and polynomial basis functions defined by the discretization:

$$p(r, z) = \sum_{i=1}^{M} p_i \chi^i(r, z), \tag{7}$$

$$\begin{bmatrix} v_r(r,z) \\ v_\theta(r,z) \\ v_z(r,z) \end{bmatrix} = \sum_{i=1}^{N} \begin{bmatrix} u_i \\ v_i \\ w_i \end{bmatrix} \Phi^i(r, z). \tag{8}$$

We use the standard mixed interpolation basis sets with continuous bilinear polynomials $\{\chi^i(r,z)\}$ for approximating pressure, and biquadratic ones $\{\Phi^i(r,z)\}$ for components of velocity.

The coefficients in (7) and (8) are determined by solving the nonlinear algebraic equations that result from the Galerkin weighted residual equations of (1) and (2). These are

$$\int_0^1 \int_0^A \chi^i(\nabla\cdot\boldsymbol{v})\, r\,\mathrm{d}r\,\mathrm{d}z = 0 \quad (i = 1,\ldots,M), \tag{9}$$

$$\int_0^1 \int_0^A \Phi^i(Re\,\boldsymbol{e}_k\cdot\boldsymbol{v}\cdot\nabla\boldsymbol{v} + \boldsymbol{e}_k\cdot\nabla p + \boldsymbol{\tau}:\nabla(\Phi^i\boldsymbol{e}_k))\, r\,\mathrm{d}r\,\mathrm{d}z = 0 \quad (k = r,\theta,z,\ i = 1,\ldots,N), \tag{10}$$

where $(\boldsymbol{e}_r, \boldsymbol{e}_\theta, \boldsymbol{e}_z)$ are the unit vectors in the cylindrical coordinate system. The $3N+M$ nonlinear equations (9) and (10) are written in a condensed form as

$$\boldsymbol{R}(\boldsymbol{x}; Re, A) = \boldsymbol{0}, \tag{11}$$

with $\boldsymbol{x}^{\mathrm{T}} \equiv (\boldsymbol{p}, \boldsymbol{u}, \boldsymbol{v}, \boldsymbol{w})^{\mathrm{T}}$ being the vector of coefficients in the finite element expansion. Starting with a first approximation to the solution vector $\boldsymbol{x}^{(0)}$ these equations are solved by Newton's method, which converges iteratively according to the sequence

$$\boldsymbol{x}^{(i+1)} = \boldsymbol{x}^{(i)} + \boldsymbol{\delta}^{(i+1)}, \tag{12}$$

where $\boldsymbol{\delta}^{(i+1)}$ is the solution of

$$\boldsymbol{J}(\boldsymbol{x}^{(i)})\,\boldsymbol{\delta}^{(i+1)} = -\boldsymbol{R}(\boldsymbol{x}^{(i)}; Re, A), \tag{13}$$

and $\boldsymbol{J}$ is the Jacobian matrix, i.e. $J_{ij} \equiv \partial R_i/\partial x_j$. Equation (13) is solved by Gaussian elimination.

Newton's method has several advantages over more simply formulated techniques for solving the set (11). Besides the rapid convergence rate to a solution, the Jacobian matrix used in (13) is the basis of computer-implemented perturbation methods for tracking families of solutions and for detecting multiple solutions in terms of changes in one or more parameters. We use the continuation procedure described in Brown, Scriven & Silliman (1980; see also Ungar & Brown 1982) to construct first approximations to solutions of (11). Intersections between two families of steady flows (simple bifurcation points) are signalled by a singular Jacobian matrix of the converged solution and are easily detected by checking the sign of the determinant of $\boldsymbol{J}$. The methods we use to force the finite-element algorithm to converge to the new bifurcating solution family and to trace flows around a limit point in Re are described in the paper of Yamaguchi, Chang & Brown (1984). The relative stability of multiple solutions to temporally monotonic disturbances in the flow is determined directly from the structure of the bifurcating families (Iooss & Joseph 1980).

The calculations presented here for liquid zones with aspect ratio of one or more were performed with a regularly spaced grid of six elements in the radial and twelve in the axial directions, which gave $3N+M = 1066$; a mesh of five radial and sixteen axial elements was used for calculations with A less than one ($3N+M = 1191$). Calculations with various coarser meshes have shown the meridional flow to be the more sensitive to element refinement than the azimuthal circulation. At least four radial and four axial biquadratic elements were found to be necessary to represent the details of a single flow cell at $A = 1$ and Reynolds numbers up to 200.

The meridional flow patterns are displayed as contours of the stream function $\Psi(r,z)$, defined by $v_r \equiv (1/r)\,\partial\Psi/\partial z$ and $v_z \equiv (-1/r)\,\partial\Psi/\partial r$, which is calculated by numerical integration of the radial velocity. All calculations were carried out in double precision arithmetic on the IBM 370/168 computer at M.I.T.

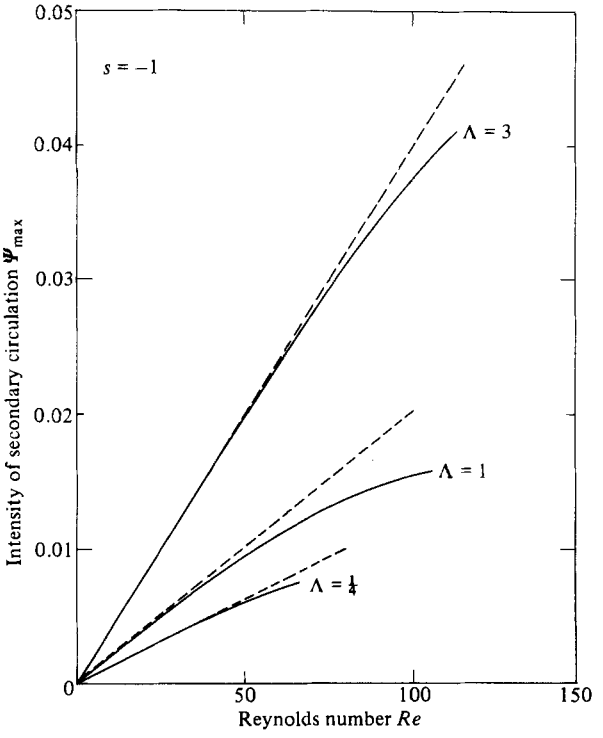

FIGURE 2. Intensity Ψ_{max} of the secondary flow for exact counter-rotation and several aspect ratios; both asymptotic (– – –) and finite-element (——) results are shown.

3. Flow structure

For low Reynolds numbers, the angular circulation was primarily a simple shear, and weak axial variation of centripetal pressure drove the slow toroidal secondary flow. In this viscous limit, the angular circulation dominated the flow and the intensity of the meridional cell scaled with Re, as described by the asymptotic analysis in I. When the disks were counter-rotated, a second toroidal cell formed as a result of the minimum in centripetal pressure that existed within the drop. This second cell emerged from the corner of the upper disk and the meniscus and grew as the degree of counter-rotation increased. When the solid disks were exactly counter-rotated ($s = -1$) the flow field was symmetric about the axial midplane of the zone.

Finite-element calculations for exact counter-rotation and $\Lambda = 1.0$ have shown the flow to be primarily viscous up to Reynolds numbers of nearly 100. For $0 \leqslant Re \leqslant 100$ the strength of the circulation increased nearly linearly with Re, the centres of the cells remained essentially stationary and the angular velocity field deformed only slightly from the uniform shear flow; each of these were properties of the perturbation solution presented in I. A quantitative comparison between the numerical and asymptotic results is shown by the intensity of the secondary circulation Ψ_{max}, which is plotted in figure 2 as a function of Re for $s = -1$ and several aspect ratios. Except for long drops ($\Lambda < 1$), the asymptotic and numerical values of Ψ_{max} agreed to within 10% up to Reynolds numbers near 100.

With other rotation ratios, the distortion of the flow field by inertial coupling occurred at lower values of the Reynolds number. For example, the streamlines and

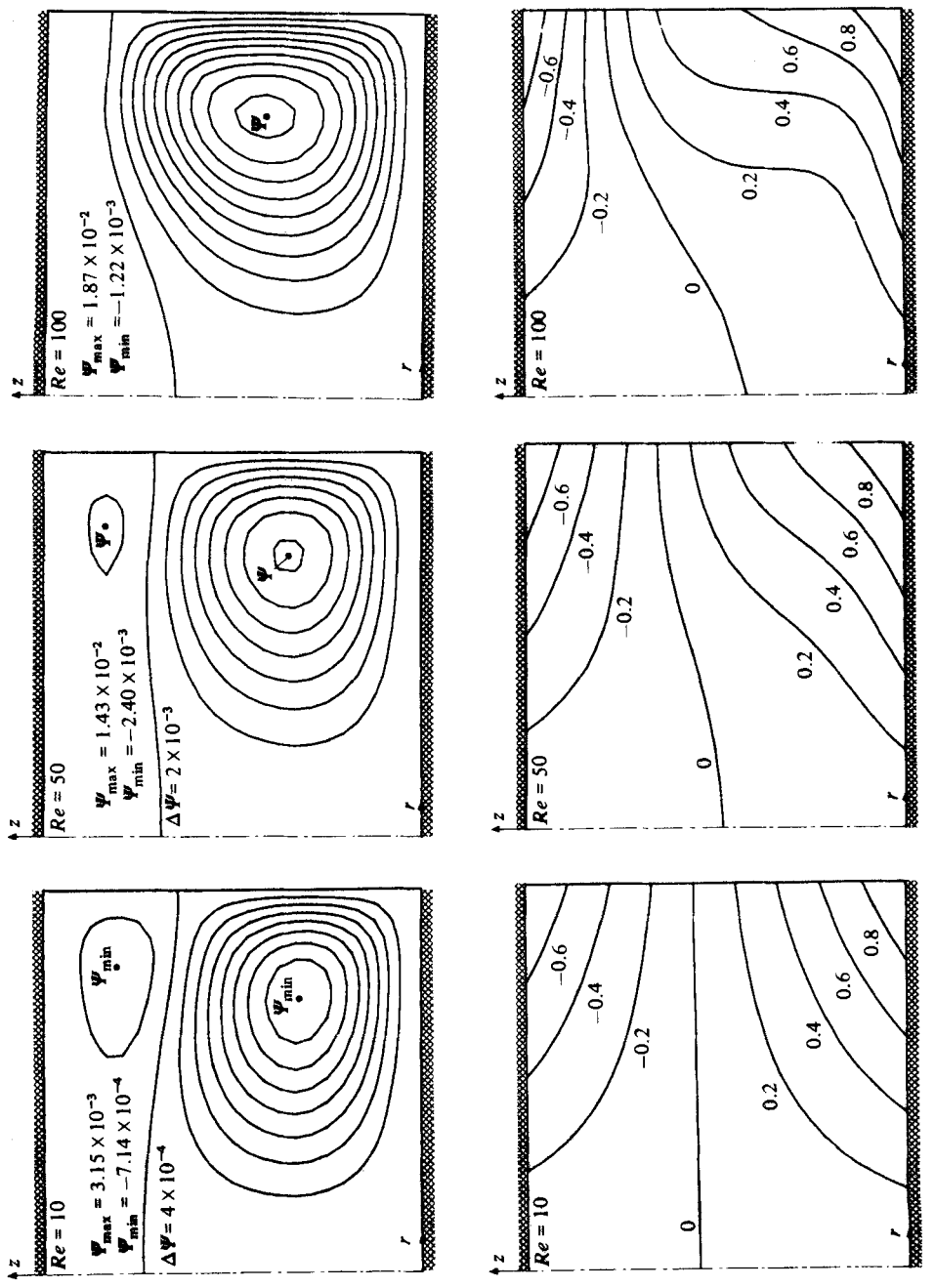

FIGURE 3. Sample streamlines and contours of azimuthal velocity for $A = 1$, $s = -\frac{1}{8}$ and several values of Reynolds number.

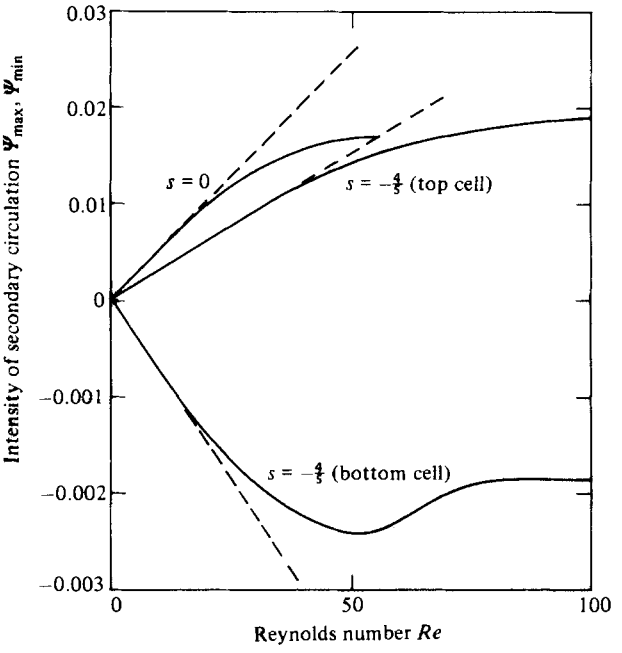

FIGURE 4. Intensity of the secondary flows for $\Lambda = 1$ and two rotation ratios; both asymptotic (– – –) and finite-element (——) results are shown.

contours of azimuthal velocity plotted in figure 3 for $s = -\frac{4}{5}$ and $\Lambda = 1$ demonstrated a significant change in the velocity field at Reynolds numbers of 50 or more. Although the flow was still primarily azimuthal, the contours of angular velocity were convected by the dominant cell upward near the meniscus and outward near the lower disk. At $Re = 100$, the flow began developing a rigidly rotating core, as marked by nearly vertical contours of angular velocity. The meridional flow was dramatically affected by the changes in centripetal pressure, and the weaker upper cell was squeezed toward the corner of the top disk and the meniscus. The intensity of the secondary circulations, as measured by $\Psi_{\min}$ and $\Psi_{\max}$, are plotted on figure 4 and show the asymptotic result to be within 10% of the finite-element calculation for Reynolds numbers up to $O(10)$. The intensity of the upper cell was greatest at $Re \approx 50$ and decreased for larger values of Re.

Pao (1970) reached a similar conclusion for analysis and calculations of the flow between rotating and stationary disks surrounded by a rotating shroud. This system is analogous to our cylindrical drop with $s = 0$, except for the boundary condition on the cylindrical sidewall. For a cylinder with $\Lambda = 1$, Pao found good agreement between finite-difference calculations and perturbation results up to $Re \approx 20$. Beyond this value $\Psi_{\max}$ levelled and reached a maximum at $Re \approx 100$.

The velocity fields for isorotation ($s = 0$) with $\Lambda = 1$ are shown in figure 5 and indicate a more subtle evolution with increasing Re. While the pattern of the cellular flow was essentially unchanged, the angular velocity developed an almost rigidly rotating core by $Re = 50$. The intensity of the secondary circulation $\Psi_{\max}$ is displayed in figure 4 and agrees with the asymptotic theory to within 10% for $Re = O(10)$.

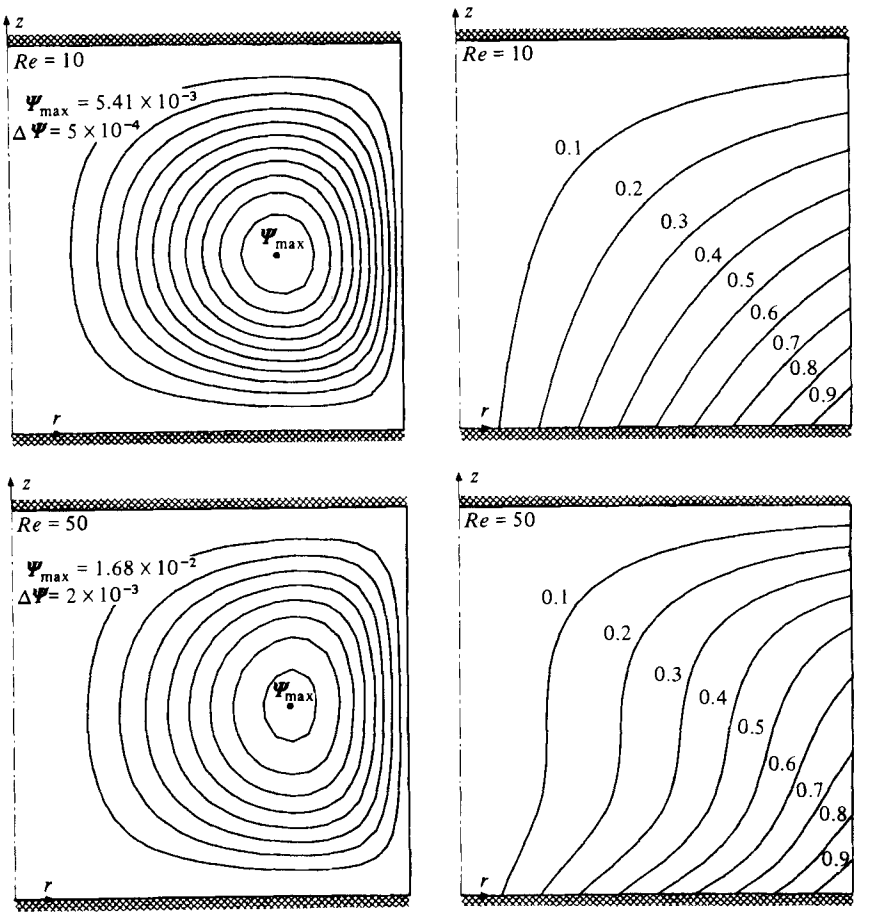

FIGURE 5. Sample streamlines and contours of azimuthal velocity for $\Lambda = 1$, $s = 0$ and several values of the Reynolds number.

4. Flow multiplicity

4.1. *Exact counter-rotation: perfect bifurcation*

Although the flows for Reynolds numbers up to 100 appeared to be dominated by viscosity, the nonlinear interactions between the rapid azimuthal velocity and the meridional circulation had important consequences for the evolution and multiplicity of the flow with increasing Re. For an exactly counter-rotated zone with $\Lambda = 1$, three families of steady axisymmetric flows were found beyond the critical Reynolds number $Re \equiv Re_c \approx 109$. These flows are represented in figure 6 by the sum of the meridional circulations for the two cells $\Psi_{min} + \Psi_{max}$; the flows in the original family had reflective symmetry about the middle of the drop and so had no net circulation. The flows in the bifurcating families did not have this symmetry; one of the cells grew larger than the other and ($\Psi_{min} + \Psi_{max} < 0$) had the larger cells at the top of the drop. The flows in the lower and upper branches at the same Reynolds number were related by a reflection about the midplane of the drop. We limit our description to flows in the upper branch only.

Elementary arguments linking simple bifurcation and the linearized stability of

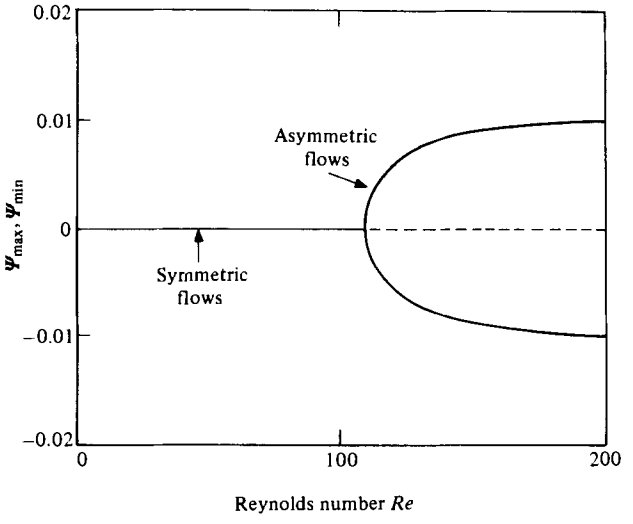

FIGURE 6. Symmetric and asymmetric flow families for $A = 1$ and $s = -1$ represented by $\psi_{max} + \psi_{min}$ and plotted as a function of Re. The dashed line – – – denotes unstable flows.

flows in the connecting families (Iooss & Joseph 1980; Yamaguchi *et al.* 1984) show that flows in both branches of the asymmetric families are stable to two-dimensional disturbances that are monotonic in time, i.e. that don't lead to time-periodic flows.

Sample velocity fields from the symmetric and lower asymmetric branch are compared in figure 7 for $A = 1$ and Reynolds numbers of 125 and 200. On the symmetric branch there was little change in the cellular flow over this range of Reynolds numbers, but the distortion of the azimuthal velocity from the meridional flow became increasingly apparent. By $Re = 200$, local minima in the angular velocity field formed halfway between the disks and the axial midplane, which seemed to presage the asymmetric flows. In the asymmetric flow, a uniformly rotating core appeared in the upper regions of the zone and the contours of angular velocity were compressed towards the lower disk. Likewise, the top cell expanded and the bottom cell contracted. Near the bifurcation point, the surfaces which separated regions of opposing azimuthal and meridional circulation lay close to the midplane of the drop. However, by $Re = 200$ both zeros of the flow had shifted roughly halfway to the lower disk at the meniscus, where the asymmetry was most pronounced. A close correspondence between these surfaces was expected near the meniscus as the non-rotating contour generated no centripetal pressure to oppose the inward flow of the meridional circulation. The secondary minima of angular velocity on the symmetric branch seen at $Re = 200$ thus indicated the possibility for asymmetric flows, although the physical mechanisms that determine the point of bifurcation may be more complex.

The finite-element/Newton algorithm was used to compute the Reynolds number Re_c for the branching of the asymmetric family for aspect ratios $0.85 \leqslant A \leqslant 3.0$. The results are displayed in figure 8, and show the most unstable aspect ratio to be approximately $A \equiv A_c \approx 1.25$. For zones with $A < A_c$, Re_c increased sharply; at $A = 0.85$ the critical Reynolds number was greater than 300, and calculations with the 5×16 element mesh were too inaccurate to warrant continuing the calculations.

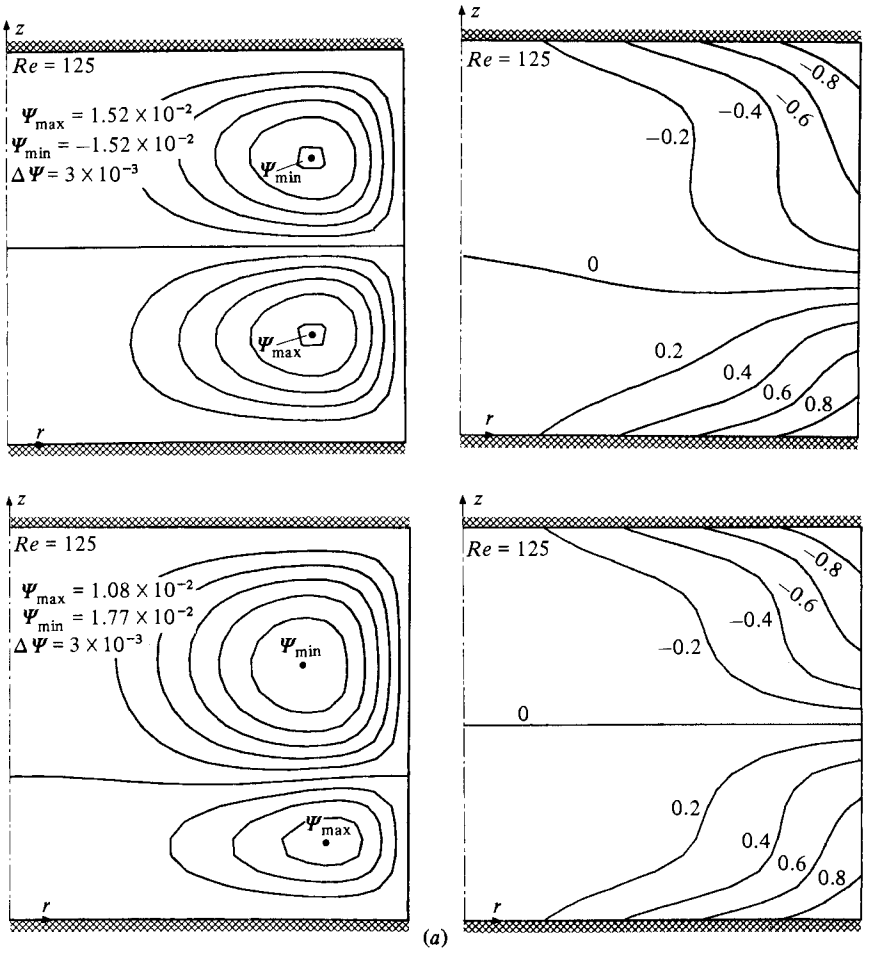

(a)

FIGURE 7(a). For description see opposite.

For zones with $\Lambda > \Lambda_c$, Re_c increased almost linearly, with $dRe_c/d\Lambda \approx 24$ as Λ was increased.

The linearity of Re_c with aspect ratio for $1.5 \leqslant \Lambda \leqslant 3.0$ suggested that for very large Λ the critical value would be extrapolated as

$$\widehat{Re} \equiv \widehat{Re}_c \approx dRe/d\Lambda = 24, \tag{14}$$

where $\widehat{Re} \equiv Re/\Lambda$ was the appropriate Reynolds number for $\Lambda \gg 1$. The result was not near the critical value of $\widehat{Re}_c = 119$ calculated by Keller & Szeto (1980; see also Szeto 1978) for the bifurcation of symmetric and asymmetric solutions to the similarity equations valid for velocity fields of the form

$$v_\theta(r, z) = rg(z), \quad \Psi(r, z) = r^2 h(z). \tag{15}$$

Asymmetric velocity fields for $s = -1$ of the form given by (15) have the separating streamline parallel to the rotating disks and displaced from the centre of the zone.

Velocity fields for members of the symmetric and asymmetric families are compared in figure 9 for $\Lambda = 3.0$ and $Re = 200$. In the symmetric flow, all but the

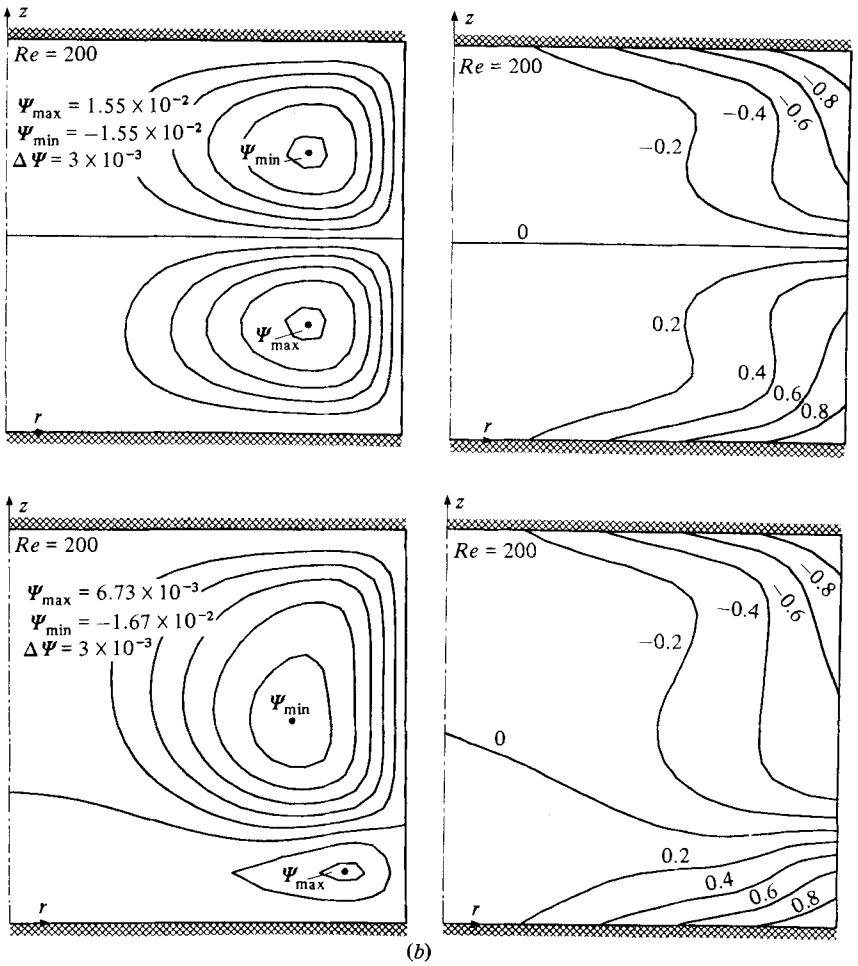

(*b*)

FIGURE 7. Comparison of velocity fields for flows belonging to the symmetric and asymmetric families at Reynolds numbers of (*a*) 125 and (*b*) 200; $A = 1$ and $s = -1$.

outer third of the flow was of the similarity form. However, the region of similarity for the asymmetric flow receded to only the inner third of the zone; the effects of the asymmetry had not reached the centreline.

4.2. *Unequal counter-rotation: imperfect bifurcation*

Changing the rotation ratio from $s = -1$ gave unequal input of angular momentum from the top and bottom surfaces, broke the axial plane of reflective symmetry that existed between the two secondary cells for exact counter-rotation and destroyed the connectivity between the families of symmetric and asymmetric flow fields. The change in structure of the flow families is described by the theory of imperfect bifurcation (Iooss & Joseph 1980). The flow fields that evolved continuously from low *Re* merged smoothly with a branch of asymmetric flows; flows in this path were all stable to disturbances that are monotonic in time. The other branch of stable asymmetric flows joined the remnants of the family of unstable symmetric flows at a limit point in *Re* and formed a sequence of flows that were isolated from the family

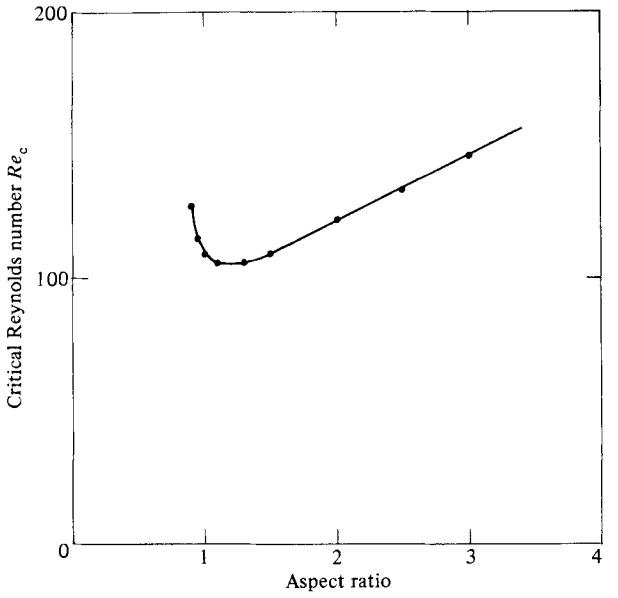

FIGURE 8. Dependence of critical Reynolds number Re_c on aspect ratio Λ.

evolving from $Re = 0$. Asymptotic theory valid for small changes in s suggested that the continuous and isolated branches of the flow shift apart rapidly, scaling as $\delta^{\frac{2}{3}}$, where δ was a measure of the deviation from exact counter-rotation.

Calculations of both flow families for $s = -0.99$ and $\Lambda = 1$ are compared to the case of exact counter-rotation ($s = -1$) in figure 10 by plotting the circulation of the lower cell $\Psi_{\max}$. Flows in the families for $s = -0.99$ were traced out by calculating flows in each family which correspond to fixed values of Re, but with changing rotation ratio to its desired value. Only changes of the order of 2×10^{-3} in s were possible for convergence of Newton's method with $Re = 200$. The solution-tracking methods described in Yamaguchi *et al.* (1984) were used to calculate the flows in both the continuous and isolated families for $s = -0.99$. The flow family that evolved from zero Re was close to the symmetric family for $s = -1$ for low values of Reynolds number and traced the upper asymmetric branch beyond the bifurcation point $Re \equiv Re_c \approx 109$. The limit point in the isolated flow family had shifted from near Re_c to $Re \approx 199$. Neither of the branches that connected at this limit point were close in the parameter space (see figure 10) to the corresponding branches for the unperturbed case. Clearly, the magnitude of this change in this position of the limit point suggested that it cannot be well approximated by an asymptotic analysis for small imperfections. The isolated family had flows where the less intense secondary cell was closest to the fastest-rotating disk and so would be difficult to achieve experimentally.

5. Discussion

Previous interpretations of experiments on small-scale floating zones (Carruthers & Grasso 1972; Fowle *et al.* 1980) have likened the rotationally driven flows to classical Taylor cells (Greenspan 1969) which are found in inertially dominated flows slightly displaced from rigid rotation. Clearly this model is not applicable to the

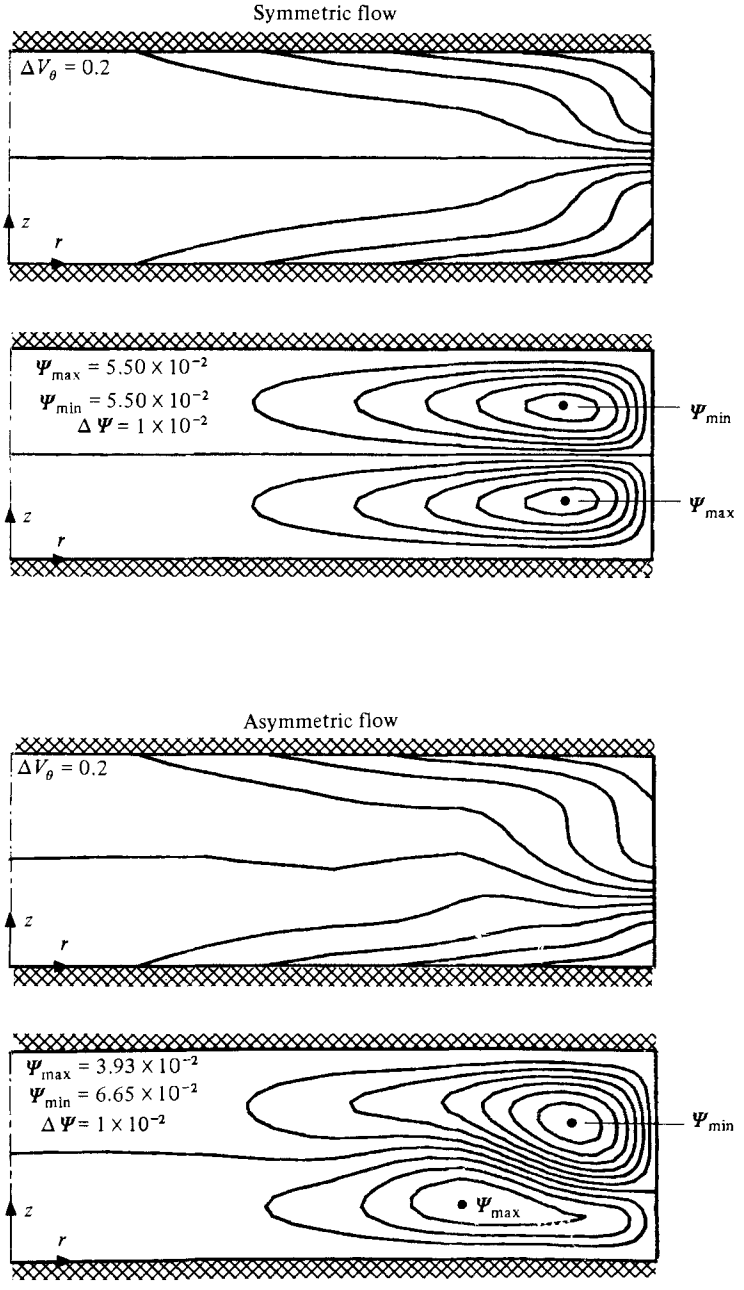

FIGURE 9. Comparison of velocity fields for flow in the symmetric and asymmetric families at $Re = 200$, $\Lambda = 3$ and $s = -1$.

floating zone at moderate Reynolds numbers ($Re < 100$), where the qualitative features of the flow are well described by the asymptotic expansion developed in I. For Reynolds numbers between 100 and 200 the flow field is still primarily viscous, but the inertial coupling between the meridional flow and the rapid angular velocity leads to multiplicity of the steady axisymmetric flows.

The bifurcation between the symmetric and asymmetric flow families reported for

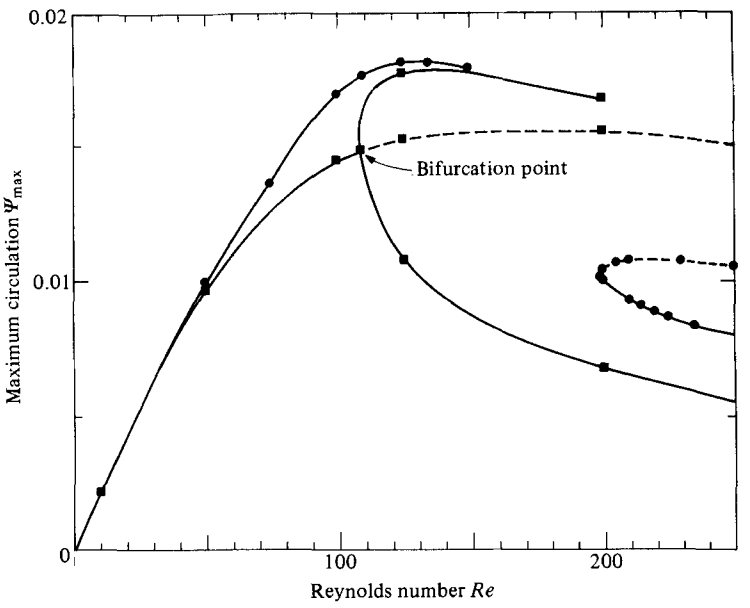

FIGURE 10. Symmetric and asymmetric flow families for $A = 1$ and rotation ratios of -1.00 (■) and -0.99 (●) represented by the circulation of the lower secondary cell Ψ_{max}. The dashed curve - - - denotes unstable flows.

perfect counter-rotation ($s = -1$) is structurally unstable (Thompson & Hunt 1973) to any small change in the system that destroys the plane of symmetry about the middle of the liquid zone. The imperfection caused by unequal rotation rates of the rods is discussed in §4.2. In the laboratory the sag of the zone caused by the action of gravity on the shape of the meniscus also will rupture the bifurcation in the same way that it affects the subcritical bifurcation which marks the Plateau–Rayleigh limit (Ungar & Brown 1982).

In contrast with the multiple solutions predicted at the Rayleigh–Plateau limit, the two asymmetric flows found for the counter-rotating cylindrical drop are both stable, at least with respect to axisymmetric disturbances that are monotonic in time. Therefore two flows may be observable for a range of Re above Re_c. The sensitivity of the flow structure to small changes in rotation ratio implies that the sharp transitions predicted for $s = -1$ will never be observed experimentally. Instead, a smooth transition between almost symmetric flows at low Re and asymmetric flows at higher values will be observed. The second family of stable flows seems isolated and is probably only accessible by specific spin-up (or down) strategies. Also, experiments by Fowle *et al.* (1980) show that non-axisymmetric flows appear suddenly in an exactly counter-rotated zone with $A = 1$ and for Reynolds numbers beyond 125 and probably mask the multiple axisymmetric flows. Careful velocity-field measurements are needed to sort out these transitions.

The inability of the similarity form of the velocity field to accurately predict the critical Reynolds number Re_c for $A = 3$ is not unexpected. The assumption that the stream function scales as r^2 is overly restrictive and neglects the role of the boundary at $r = A$ on setting the form of the returning flow. Brady (1981, 1983) has documented the failure of the similarity solution for $s = 0$ and large, but finite, A by comparison with solution of the boundary-layer equations. He found the similarity solution to

first fail at the edge of the disks and the region of validity to shrink to the centreline with increasing Re. A corresponding effect has been reported in rotating flows of viscoelastic fluids (Griffiths, Jones & Walters 1969; Kramer & Johnson 1972; Hill 1972). Here elastic stresses in the flow can reverse the direction of the rotationally driven meridional flow near the outer edge of the zone. The similarity form, which does not allow for this edge effect, fails everywhere when the elasticity is increased so that the reverse flow reaches the centreline.

This same type of breakdown in the similarity form of a solution has been observed in other problems with reverse flow (Brady & Acrivos 1981). We have not made a detailed comparison between our results and the similarity flow; however, the streamlines displayed in figure 9 show that asymmetry in the flows in the bifurcating family indeed originate at the meniscus.

Although we have not searched for analogues of the other 16 solution families detected for the similarity equations (Szeto 1978), it can be argued that some of these indeed exist for the cylindrical drop. The problems of a cylindrical drop for $\Lambda \gg 1$ with either a shear-free interface ($\alpha = 1$) at $r = \Lambda$ or a boundary on which the velocity field fits a known similarity solution ($\alpha = 0$) ($g(z; Re)$, $h(z; Re)$) are limits in the sequence of problems defined in terms of α, $0 \leqslant \alpha \leqslant 1$, by the boundary conditions

$$(1-\alpha)\, v_\theta(\Lambda, z) + \alpha \frac{\partial v_\theta}{\partial r} - (1-\alpha)\, \Lambda\, g(z; Re) = 0, \tag{16a}$$

$$v_r(\Lambda, z) - \Lambda(1-\alpha)\, h'(z; Re) = 0, \tag{16b}$$

$$(1-\alpha)\, v_z(\Lambda, z) - \alpha \frac{\partial v_z}{\partial r} + (1-\alpha)\, 2h(z; Re)\, \Lambda = 0, \tag{16c}$$

where the prime denotes differentiation with respect to z. At $\alpha = 0$, each of the similarity flows of Szeto (1978) is a solution of the equations of motion with the boundary condition (16) and the functions $g(z; Re)$ and $h(z; Re)$ picked to match. The sequence of problems defined by varying α to unity gives a method for calculating the analogous solutions for the drop with a shear-free interface, if they exist.

This research was supported by the Microgravity Science and Applications Division of the U.S. National Aeronautics and Space Administration and by the Information Processing Center at M.I.T. The authors are grateful to J. F. Brady for valuable discussions concerning the validity of similarity solutions.

REFERENCES

Brady, J. F. 1981 On the flow between two finite rotating disks. *Bull. Am. Phys. Soc.* **26**, 1269.

Brady, J. F. 1983 On the flow between stationary and rotating finite disks. Submitted to *J. Fluid Mech.*

Brady, J. F. & Acrivos, A. 1982 Closed-cavity laminar flows at moderate Reynolds number. *J. Fluid Mech.* **115**, 427–442.

Brown, R. A., Scriven, L. E. & Silliman, W. J. 1980 Computer-aided analysis of nonlinear problems in transport phenomena. In *New Approaches to Non-linear Problems in Dynamics* (ed. P. J. Holmes). SIAM.

Carruthers, J. R. & Grasso, M. 1972 Studies of floating zones in simulated zero gravity. *J. Appl. Phys.* **43**, 436–443.

Fowle, A. A., Soto, L., Strong, P. F. & Wang, C. A. 1980 Experimental and flow characteristics of floating liquid columns confined between rotating disks. *Final Rep. to NASA, Washington, D.C., Contract* NASW-3186 *by Arthur D. Little.*

GREENSPAN, H. P. 1969 *The Theory of Rotating Fluids.* Cambridge University Press.

GRIFFITHS, D. E., JONES, D. T. & WALTERS, K. 1969 A flow reversal due to edge effects. *J. Fluid Mech.* **36**, 161–175.

HARRIOTT, G. M. & BROWN, R. A. 1983 Flow in a differentially rotated cylindrical drop at low Reynolds number. *J. Fluid Mech.* **126**, 269–285.

HILL, C. T. 1972 Nearly viscometric flow of viscoelastic fluids in the disk and cylinder system. II: Experimental. *Trans. Soc. Rheol.* **16**, 213–245.

HOLODNIOK, M., KUBIČEK, M. & HLAVAČEK, V. 1981 Computation of the flow between two rotating coaxial disks: multiplicity of steady-state solutions. *J. Fluid Mech.* **108**, 227–240.

HUYAKORN, P., TAYLOR, C., LEE, R. & GRESHO, P. 1978 A comparison of various mixed-interpolation finite elements in the velocity–pressure formulation of the Navier–Stokes equations. *Comp. Fluids* **6**, 25–35.

IOOSS, G. & JOSEPH, D. D. 1980 *Elementary Stability and Bifurcation Theory.* Springer.

KÁRMÁN, T. VON 1921 Über laminare und turbulente Reibung. *Z. angew. Math. Mech.* **1**, 233–251.

KEENER, J. P. & KELLER, H. B. 1973 Perturbed bifurcation theory. *Arch Rat. Mech. Anal.* **50**, 159–175.

KELLER, H. B. & SZETO, R. K.-H. 1980 Calculation of flows between rotating disks. In *Computing Methods in Applied Sciences and Engineering* (ed. R. Glowinski & J. L. Lions). North-Holland.

KOBAYASKI, N. & WILCOX, W. R. 1982 Computational studies of convection due to rotation in a cylindrical floating zone. *J. Crystal Growth* **59**, 616–624.

KRAMER, J. M. & JOHNSON, M. W. 1972 Nearly viscometric flow in a disk and cylinder system. I: Theoretical. *Trans. Soc. Rheol.* **16**, 197–212.

KUBIČEK, M., HOLODNIOK, M. & HLAVAČEK, V. 1976 Calculation of flow between two rotating coaxial disks by differentiation with respect to an actual parameter. *Comp. Fluids* **4**, 59–64.

MATKOWSKY, B. J. & REISS, E. L. 1977 Singular perturbation of bifurcations. *SIAM J. Appl. Maths* **33**, 230–255.

NGUYEN, N. D., RIBAULT, J. P. & FLORENT, P. 1975 Multiple solutions for flow between coaxial disks. *J. Fluid Mech.* **68**, 369–388.

PAO, H.-P. 1970 A numerical computation of a confined rotating flow. *Trans. ASME* E: *J. Appl. Mech.* **37**, 480–487.

PEARSON, C. E. 1965 Numerical solutions for the time-dependent viscous flow between two rotating coaxial disks. *J. Fluid Mech.* **21**, 623–633.

ROBERTS, S. M. & SHIPMAN, J. S. 1976 Computation of the flow between a rotating and a stationary disk. *J. Fluid Mech.* **73**, 53–63.

SZETO, R. K.-H. 1978 The flow between rotating coaxial disks. Ph.D. thesis, California Institute of Technology.

THOMASSET, F. 1981 *Implementation of Finite Element Methods for Navier–Stokes Equations.* Springer.

THOMPSON, J. M. T. & HUNT, G. W. 1973 *A General Theory of Elastic Stability.* Wiley.

UNGAR, L. H. & BROWN, R. A. 1982 The dependence of the shape and stability of captive rotating drops on multiple parameters. *Phil. Trans. R. Soc. Lond.* A **306**, 347–370.

YAMAGUCHI, Y., CHANG, C. J. & BROWN, R. A. 1984 Multiple buoyancy-driven flows in a vertical cylinder heated from below. *Phil. Trans. R. Soc. Lond.* (in press).